MATERIALS CHEMISTRY FRONTIERS

RESEARCH ARTICLE

View Article Online
View Journal | View Issue

Cite this: *Mater. Chem. Front.*, 2026, **10**, 72

Improving the phosphorescence properties of doped materials through the heavy atom effect of the hosts

Xiyao Xu,†[a] Peng Chen,†[b] Yuping Xia,†[a] Wenbin Hui,[c] Heqi Gao,*[c] Shihao Luo,[a] Wenbo Dai,[b] Junbo Zhong,[a] Yunxiang Lei *[b] and Yan Chen*[d]

Using a host–guest doping strategy to construct materials with excellent phosphorescence properties has important practical significance, and designing guests with strong luminescence properties to enhance the phosphorescence activity of doped systems is a commonly used method. However, enhancing phosphorescence performance through hosts is often overlooked. Herein, a doped system was constructed by selecting five compounds containing Group 15 elements (triphenylamine, triphenylphosphine, triphenylarsine, triphenylstibine, and triphenylbismuthine) as the hosts, and triphenylamine derivatives as the guests. The luminescence intensity of the doped materials is significantly enhanced by the external heavy atom effect of the hosts, and the phosphorescence quantum efficiency gradually increases from 5.2–5.6% in triphenylbismuthine-based doped materials to 22.8–26.0% in triphenylbismuth-based doped materials. Theoretical calculations show that heavy atoms significantly enhance the SOC of the hosts, thereby inducing an increase in the phosphorescence intensity of the doped materials. In addition, the single crystal structure and XRD analyses of the hosts further demonstrated that heavy atoms give the host a larger spatial volume and good deformability, allowing for better encapsulation of guest molecules. Finally, the doped materials can be effectively used for *in vivo* subcutaneous afterglow imaging in mice, demonstrating good imaging performance.

Received 30th August 2025,
Accepted 1st November 2025

DOI: 10.1039/d5qm00645g

rsc.li/frontiers-materials

Introduction

Organic or metal–organic room temperature phosphorescent (RTP) materials have shown great potential for application in fields such as information encryption storage, flexible device displays, and biological diagnosis and treatment due to their luminescence diversity, long luminescence lifetime, and excellent biocompatibility.[1–8] There are two key factors that directly determine whether phosphorescent materials have high phosphorescence activity. One factor is promotion of the intersystem crossing (ISC) process of excitons from singlet to triplet states,[9–12] and the other is maximizing the suppression of non-radiative transitions of triplet excitons.[13–16] The ISC process of excitons is a prerequisite for organic/metal–organic materials to show phosphorescence emission and long afterglow,[17–19] while suppressing the non-radiative transition rate of excitons is the key to improving the phosphorescence emission intensity.[20–22] But for most luminescent materials, the lack of heavy atoms leads to weak spin–orbit coupling of molecules, so the singlet excitons face severe transition barriers. In addition, the thermal motion of molecules consumes exciton energy, which further hinders the ordinary organic/metal organic materials to have RTP activity. Although some metal–organic complexes have phosphorescence properties, most of them rely on precious platinum and iridium elements. To achieve phosphorescence activity of organic/metal–organic materials at room temperature, some methods have gradually been proposed, such as the heavy atom effect, hydrogen/ionic bonding, engineering, supramolecular assembly, and host–guest doping.[23–27] Among these emerging strategies, the host–guest doping strategy has attracted widespread attention due to the low content of the guest reducing economic costs, the diverse molecular types broadening the doped systems, and the special interactions between the host and guest regulating the phosphorescence properties.[28–31] In most doped systems, the phosphorescence essentially comes from guest molecules,

[a] *Department of Bum and Plastic Surgery, Zigong Fourth People's Hospital, Zigong 643099, China*
[b] *School of Chemistry and Materials Engineering, Wenzhou University, Wenzhou 325000, China. E-mail: yunxianglei@wzu.edu.cn*
[c] *School of Chemistry, Engineering Research Center of Energy Storage Materials and Devices, Ministry of Education, Xi'an Key Laboratory of Sustainable Polymer Materials, Xi'an Jiaotong University, Xi'an 710049, China. E-mail: gaoheqi@xjtu.edu.cn*
[d] *Quzhou Hospital Affiliated to Wenzhou Medical University, Quzhou 324000, China. E-mail: qzchenyan@wmu.edu.cn*
† These authors contributed equally.

so enhancing the luminescence performance of the guest is a common strategy to improve the phosphorescence properties of doped materials.[32–35] For example, increasing the conjugation degree of guest molecules to prolong the phosphorescence wavelength of doped materials,[32] or quaternization of guest molecules containing heteroatoms to enhance the phosphorescence emission intensity of doped materials.[33] However, in addition to the well-known rigid role of the host in suppressing the movement of guest molecules, the use of the host's heavy atom effect to enhance the phosphorescence intensity of doped materials is often overlooked. Although there have been reports on utilizing the external heavy atom effect of the host to enhance the phosphorescence properties of doped materials, most of them still rely on halogen atoms.[36–40] Developing new hosts with heavy atoms can enrich the phosphorescence systems and provide more choices for constructing doped materials with excellent phosphorescence properties. Triphenylamine (**TPA**),[41] triphenylphosphorus (**TPP**),[42] and triphenylarsenic (**TPAs**),[42] and especially **TPA,** have been proven to be excellent host molecules. The other two metal organic compounds (triphenylantimony (**TPSb**) and triphenylbismuthine (**TPBi**)) containing pnictogens also have good properties as hosts such as low-melting point, easy crystallization, low cost and availability.

In this work, we used the above five compounds (**TPA**, **TPP**, **TPAs**, **TPSb**, and **TPBi**) as the hosts, and then introduced a neutral phenyl group (**DBA**), an electron donating amino group (**MADBA**), and an electron withdrawing fluorine atom (**FDBA**) into triphenylamine to obtain three triphenylamine derivatives as the guests. The experimental results show that regardless of which guest molecules were doped in the five hosts, the phosphorescence intensity of the doped materials will be significantly enhanced, and the phosphorescence quantum yield (QY) gradually increased from 5.2–5.6% to 22.8–26.0%, with an increase of 4.4–4.6 times, indicating the significantly enhanced phosphorescence emission due to the external heavy atom effect of the hosts. Additionally, it is rare that the phosphorescence lifetime can still be maintained from 65–208 ms in **TPA**-based doped materials to 190–258 ms in **TPSb**-based doped materials. Theoretical calculations show that the SOC constants of the hosts have increased from 1.1 in **TPA** to 285 in **TPSb**, with a 259-fold increase, further indicating that the heavy atoms of the hosts play a significant role in enhancing the ISC process of excitons. In addition, the single crystal structure analysis showed that as the atomic radius increases, the intermolecular distances and spatial volumes of hosts also gradually increase, and the XRD curves further show that the deformation ability of the host also gradually increases, which is beneficial for the host matrix to better encapsulate the guest molecules. Finally, the doped material **MADBA/TPP** NPs was successfully used for subcutaneous injection in mice, with a signal to background ratio (SBR) of 28.2. This work successfully enhanced the phosphorescence activity of the doped systems by the external heavy atom effect of hosts, providing a new strategy for constructing doped materials with good phosphorescence properties.

Results and discussion

The guest molecules **DBA**, **FDBA** and **MADBA** were synthesized following the reported method (Fig. 1a and Scheme S1). The

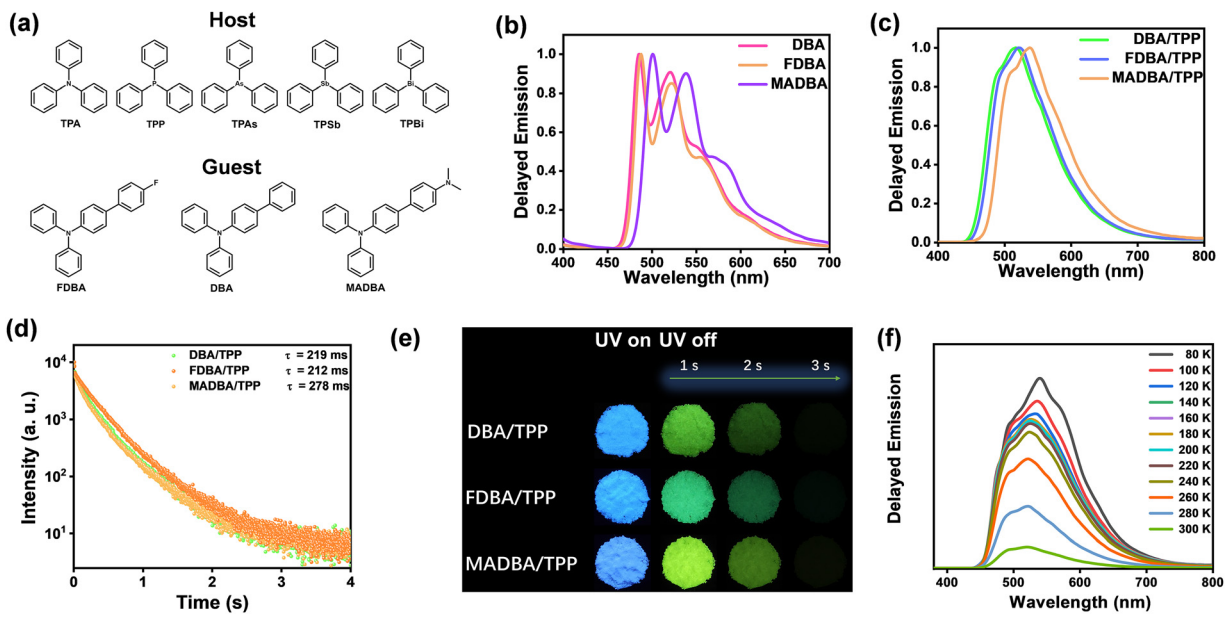

Fig. 1 (a) Molecular structures of the guest and host molecules. (b) Phosphorescence spectra of the guests **DBA**, **FDBA**, and **MADBA** (solvent: tetramethyltetrahydrofuran, concentration: 1.0×10^{-5} mol L^{-1}, 77 K; Ex. wavelength: 340 nm, delayed time: 0.1 ms). (c) Phosphorescence spectra of the doped materials **DBA/TPP**, **FDBA/TPP** and **MADBA/TPP** (solid state, Ex. wavelength: 340 nm, delayed time: 0.1 ms). (d) Phosphorescence decay curves of doped materials **DBA/TPP**, **FDBA/TPP** and **MADBA/TPP** (solid state, Ex. wavelength: 340 nm). (e) Luminescence photographs of the doped system. (f) Phosphorescence spectra of the doped material **DBA/TPP** at different temperatures (solid state, Ex. wavelength: 340 nm, delayed time: 0.1 ms).

molecular structures and purities were verified using nuclear magnetic resonance spectroscopy and high-performance liquid chromatography (Fig. S1). Three guests all exhibit strong blue fluorescence emission in the solution state, with the emission wavelength of 380–395 nm (Fig. S2), and the fluorescence QY is as high as 42.8%, 46.3%, and 50.6%, respectively. In addition, the guests display a greenish green afterglow at low temperature (77 K), with the phosphorescence wavelength of 521–539 nm (Fig. 1b), and the phosphorescence lifetime is 864–956 ms (Fig. S3). The above results show that the three guests have similar optical properties, which may be due to the weak electron withdrawing ability of the F atom, resulting in unobvious intramolecular charge transfer of guest **FDBA**. The UV-absorption spectra also further displayed that the absorption wavelengths of three guests differ by only 16 nm (Fig. S4). Next, we chose **TPP** as the host to construct doped materials, and the doped materials were fabricated by the melt-casting method. Given that the host–guest doping ratio will influence the phosphorescence emission intensity of doped materials,[43] the materials **MADBA/TPP** with varying molar ratios (1 : 50 to 1 : 100 000) were prepared, and the results showed that the guest-to-host molar ratio of 1 : 1000 can be adopted for the doped system (Fig. S5). Therefore, this ratio has been chosen for the doped materials (**DBA/TPP**, **FDBA/TPP**, and **MADBA/TPP**) as the research targets. Three doped materials all display strong blue fluorescence with a wavelength of 388–397 nm under a UV-lamp (Fig. 1e and Fig. S6), and exhibited a green afterglow for 2–3 s after removing the excitation source (Fig. 1e), indicating that the materials have RTP activity. The delayed emission spectra of **DBA/TPP** at various temperatures from 80 to 300 K showed that the emission intensity gradually decreased as the temperature increased, further demonstrating that the afterglow was phosphorescence rather than thermally activated delayed fluorescence (Fig. 1f). The phosphorescence wavelength is 517–538 nm (Fig. 1c), the phosphorescence lifetime is 212–278 ms (Fig. 1d), and the phosphorescence QY is 6.0%, 6.2%, and 6.3%, respectively. The above results indicate that the doped systems with three different guests in the same host show a similar phosphorescence performance.

Next, we will focus on studying the effects of five host compounds containing N, P, As, Sb, and Bi atoms (triphenylamine (**TPA**), triphenylphosphine (**TPP**), triphenylarsine (**TPAs**), triphenylstibine (**TPSb**), and triphenylbismuthine (**TPBi**)) on the luminescence properties of doped materials with the same guest. The molecular structures and purities of the five host compounds were verified using single crystal structures, NMR spectra, and high-performance liquid chromatography (Fig. 3b and Fig. S7). In addition, all five hosts have good thermal stability, and their decomposition temperature is greater than 105 °C (Fig. S8). Five hosts have no phosphorescence activity at room temperature (Fig. S9), and **MADBA** was selected as the guest to construct five doped materials. All doped materials show similar bright blue fluorescence with a fluorescence QY of 36.6–45.5% (Fig. 2e and Table S1). After turning off the excitation light, all materials show a green afterglow with a phosphorescence wavelength of approximately 538 nm (Fig. 2a and e),

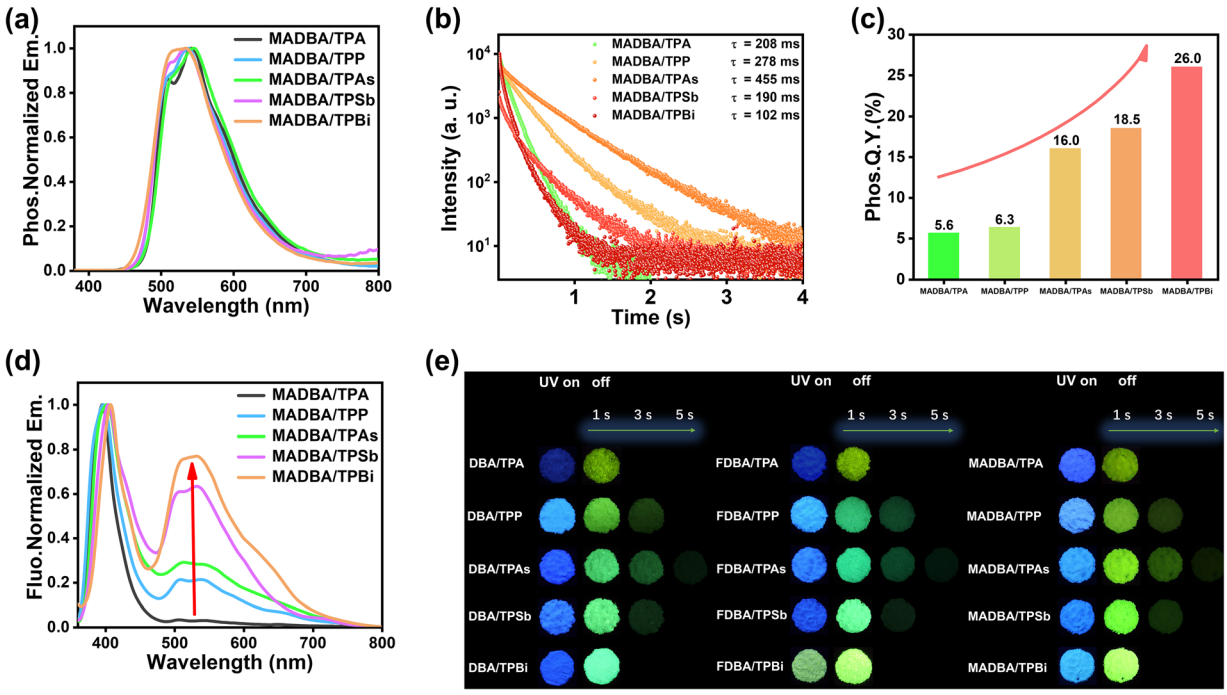

Fig. 2 (a) Phosphorescence spectra of the five **MADBA**-based doped materials (solid state, Ex. wavelength: 340 nm, delayed time: 0.1 ms). (b) Phosphorescence decay curves of the five doped materials (solid state, Ex. wavelength: 340 nm). (c) Phosphorescence QYs of the five doped materials (solid state). (d) Steady-state emission spectra of the five **MADBA**-based doped materials (solid state, Ex. wavelength: 340 nm). (e) Luminescence photographs of the doped system.

and the lifetime is 102–455 ms (Fig. 2b). However, as the molecular weight of the guests gradually increases, the afterglow brightness of the corresponding doped materials gradually increases from weak to strong (Fig. 2e), and the phosphorescence QY also gradually increased from 5.6% in **MADBA/TPA** to 26.0% in **MADBA/TPBi** (Table S1 and Fig. 2c), an increase of up to 4.6 times. The changes in phosphorescence intensity are also clearly reflected even in steady-state spectra. As shown in Fig. 2d, the doped materials show two emission peaks at 398 nm and 538 nm, with the former being the fluorescence emission and the latter being the phosphorescence emission. Surprisingly, the emission intensity of the materials at 538 nm gradually significantly increased from **MADBA/TPA** to **MADBA/TPBi**, with an enhancement factor of 27.8. The above results confirmed that the heavy atom effect of the hosts directly promotes the enhancement of the phosphorescence intensity in doped materials. For other two groups of doped materials with **DBA** and **FDBA** as the guests, the hosts also play the same role. For the **DBA**-based doped system, the difference in fluorescence intensity is small, the fluorescence quantum efficiency is 33.7–40.5% (Table S1), and the fluorescence emission wavelength is 381–395 nm (Fig. S10). But the phosphorescence emission intensity also gradually increases, the phosphorescence QY obviously gradually increases from 5.2% to 22.8% (Table S1), the phosphorescence wavelength remains basically unchanged at 523 nm (Fig. S11), and the phosphorescence lifetime is 68–539 ms (Fig. S12). Another group of **FDBA**-based doped materials also follows a similar pattern, with similar fluorescence properties but gradually increasing phosphorescence intensity (Table S1 and Fig. S13–S15). The above results clearly indicate that the external heavy atom effect of the hosts has universality and can have the same phosphorescence enhancement effect on different guests.

Heavy atoms in substances can effectively increase the SOC of molecules, thereby promoting the production of phosphorescence emission.[44,45] The hosts containing heavy atoms such as arsenic, bismuth, and tellurium in this doped system can play an external heavy atom effect, which facilitates the ISC process of guest excitons. The calculation results also conformed to this theory. The SOC between the S_1 state and the T_1 state of five hosts gradually increased from 1.1 cm^{-1} to 9.6 cm^{-1} to 35.7 cm^{-1} to 128.7 cm^{-1} to 285.8 cm^{-1}, the increase of up to 259 times, and the other SOC between the S_1 state and the Tn states of five hosts also significantly increased (Fig. 3a). Such a large SOC obviously helps improve the ISC efficiency of excitons, endowing the doped materials with better phosphorescence activity. Subsequently, we calculated the values of k_{ISC} (rate

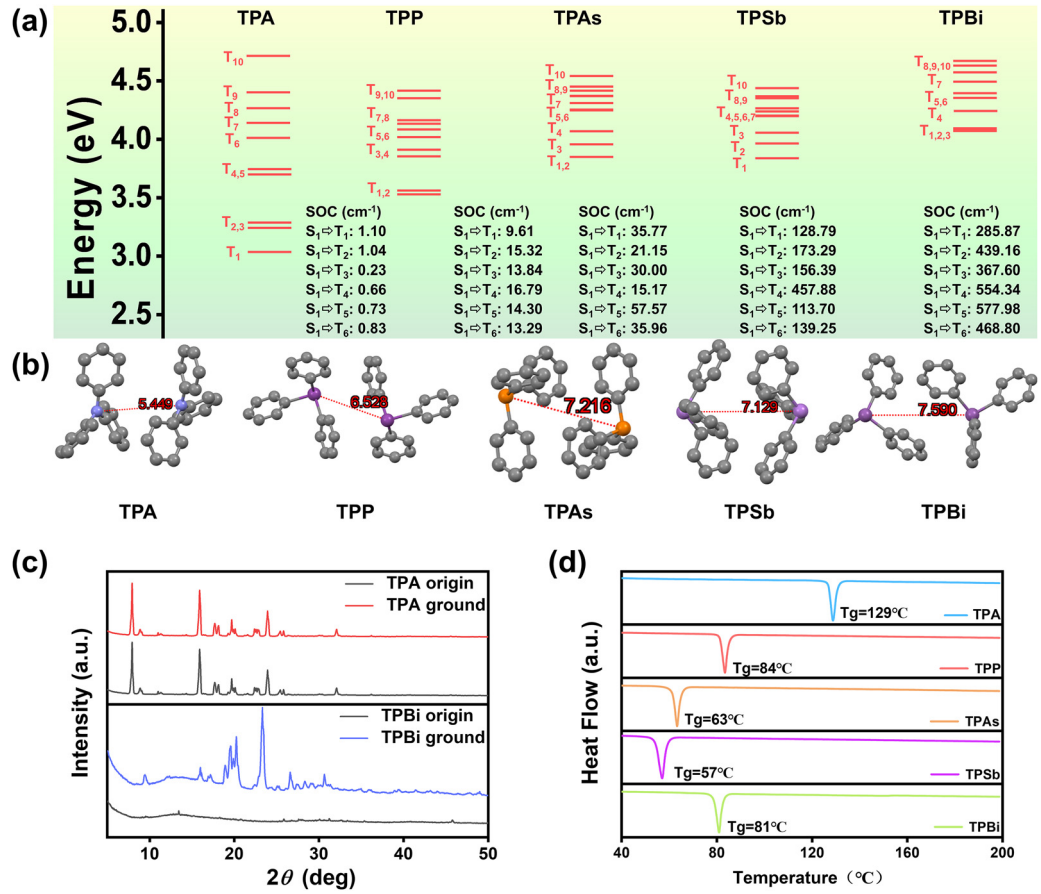

Fig. 3 (a) SOC and energy levels of five hosts. (b) Single-crystal structures of five hosts (from https://doi.org/10.1002/adfm.202108072, https://doi.org/10.5517/ccdc.csd.cc2p8ygd, https://doi.org/10.5517/ccdc.csd.cc2p8yhf, and https://doi.org/10.5517/ccdc.csd.cc2p8yjg). (c) XRD curves of **TPA** and **TPBi** in different states. (d) DSC curves of five hosts.

Table 1 Photophysical properties of the doped materials[a]

Sample	τ_F [ns]	τ_P [ms]	Φ_P [%]	k_{ISC} [s^{-1}]	k_r^P [s^{-1}]
MADBA/TPA	5.04	208	5.6	1.11×10^7	0.27
MADBA/TPP	4.98	278	6.3	1.27×10^7	0.23
MADBA/TPAs	5.22	455	16.0	3.07×10^7	0.35
MADBA/TPSb	5.40	190	18.5	3.42×10^7	0.97
MADBA/TPBi	4.88	102	26.0	5.32×10^7	2.54

[a] Note: guest : host = 1 : 1000 (molar ratio). k_{ISC} is the rate constant of ISC and k_r^P is the radiative rate constant of phosphorescence. $k_{ISC} = \Phi_P/\tau_F$; $k_r^P = \Phi_P/\tau_P$.

constant of ISC) and k_r^P (radiative rate constant of phosphorescence). The calculation results show that from **MADBA/TPA** to **MADBA/TPBi**, as the mass of atoms contained in the host gradually increases, the values of k_{ISC} and k_r^P also gradually increase, k_{ISC} increased by 4.80 times and k_r^P increased by 9.41 times (Table 1). This also indicates that the heavy atoms contained in the hosts can effectively increase the phosphorescence emission intensity of the doped materials. In addition, in most doped systems, the host matrix needs to change the morphology to encapsulate guest molecules, thereby suppressing their thermal motion.[46,47] As the radius of the atom increases, the intermolecular distances of hosts weaken, leading to an increase in deformability. XRD spectra show that compared to **TPA** and **TPP**, the morphology of the three hosts **TPAs**, **TPSb** and **TPBi** is more prone to change (Fig. 3c and Fig. S16). Further analysis of the single crystal structures of the five hosts also confirmed that the intermolecular distances of the five host molecules gradually increase, from 5.4 Å to 7.6 Å (Fig. 3b). The long distances lead to a weakening of intermolecular interactions and an increase in the spatial volume of molecules. In addition, the DSC results show that the melting points of the five main groups gradually

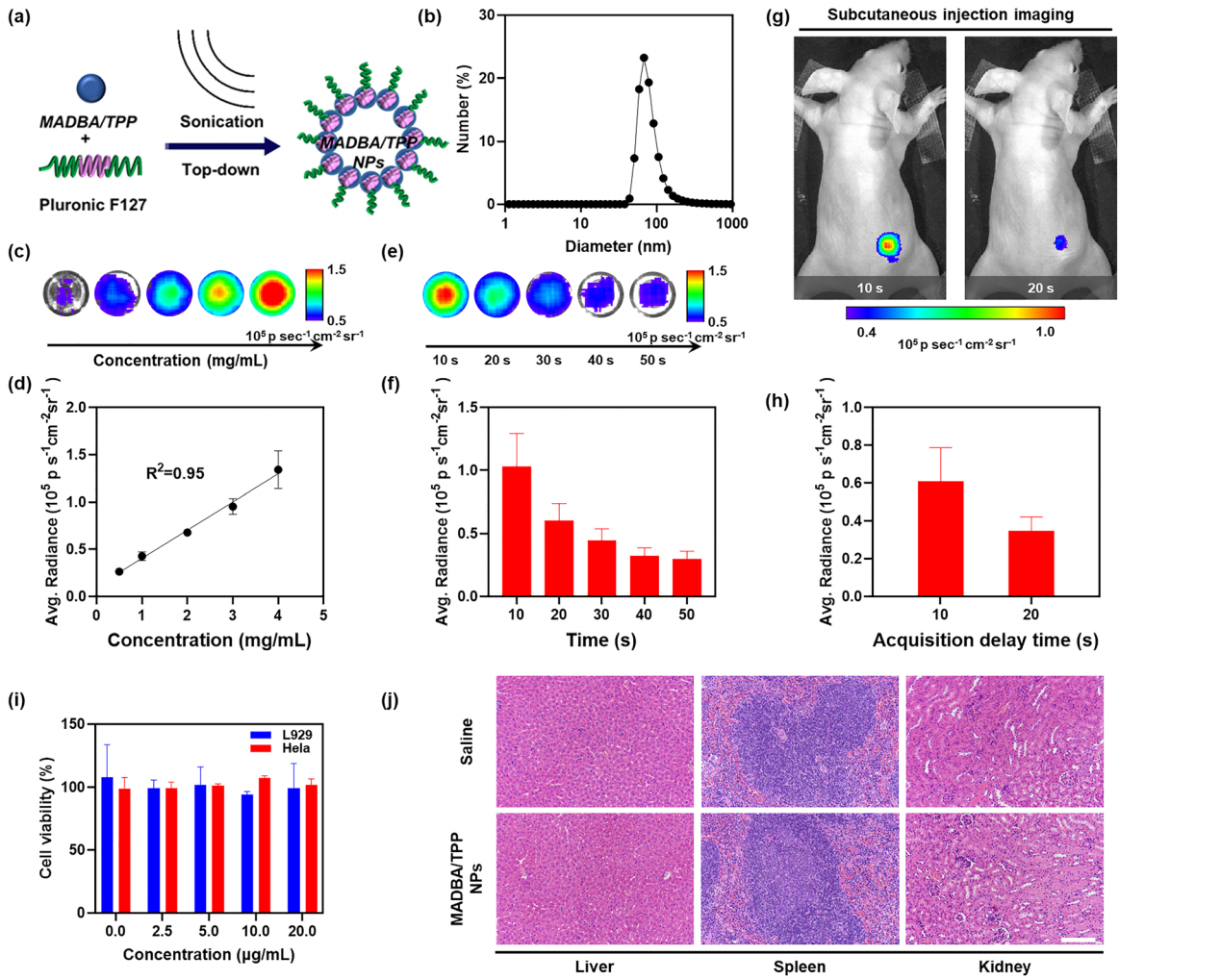

Fig. 4 (a) Schematic illustration of the preparation of **MADBA/TPP** NPs. (b) Hydrodynamic diameter of **MADBA/TPP** NPs determined by DLS. (c) and (d) Representative images (c) of phosphorescent signals with increasing concentration of **MADBA/TPP** NPs solution, along with the corresponding linear relationship plot (d) (error bars, n = 3). (e) and (f) Representative images (e) and plots (f) of the time-dependent phosphorescence decay of **MADBA/TPP** NPs recorded after the UV irradiation was turned off. (g) Subcutaneous afterglow imaging of mice (NPs: 50 μL, 4 mg mL^{-1}; Ex.: 365 nm). (h) Quantitative analysis based on the typical phosphorescence signal images in (g). (i) Cell viability of L929 cells and HeLa cells after 24-hour co-incubation with MADBA/TPP NPs at different concentrations. (j) Representative H&E-stained images of the liver, spleen, and kidneys from BALB/c mice at 7 days after intravenous injection of physiological saline and MADBA/TPP NPs (NPs: 50 μL, 4 mg mL^{-1}), respectively.

decreased from 129 °C to 57 °C (Fig. 3d), further indicating that as the atomic radius of the Group 15 elements increased, the intermolecular interactions between the host weakened.

Given the long luminescence lifetime of phosphorescence materials, which can effectively avoid interference from tissue self-luminescence, they have natural advantages in bioimaging.[48,49] Therefore, phosphorescent nanoparticles were prepared for afterglow imaging by encapsulating **MADBA/TPP** nanoparticles (NPs) with amphiphilic copolymer F127 as the matrix using the nanoprecipitation method (Fig. 4a). Dynamic light scattering (DLS) was performed to determine the size of the NPs and the results show that the NPs exhibited a mean hydrodynamic diameter of approximately 74 nm (Fig. 4b). Subsequently, we acquired afterglow imaging images and phosphorescence intensities of **MADBA/TPP** NPs at different concentrations (0.5, 1, 2, 3, and 4 mg mL^{-1}) under the same conditions using the bioluminescence mode of IVIS Lumina II (Fig. 4c). The results demonstrated that the phosphorescence intensity of **MADBA/TPP** NPs increased linearly with the increase in their solution concentration (Fig. 4d), implying their potential for quantitative analysis. Next, we also recorded the phosphorescence signal decay of **MADBA/TPP** NPs (Fig. 4e). The results showed that distinguishable phosphorescence signals could still be detected even 50 seconds after the removal of UV irradiation, confirming their potential for afterglow bioimaging (Fig. 4f). Therefore, we injected **MADBA/TPP** NPs (4 mg mL^{-1}) subcutaneously into mice for afterglow imaging (Fig. 4g and h). All animal experiments were approved by the Animal Ethics Committee of Wenzhou University (issue no. WZU-2025-018), and performed in compliance with the guidelines of the Institutional Animal Care and Use Committee of Wenzhou University. All BALB/c nude mice (average weight 16–22 g) were purchased and acclimatized to the animal facility for one week prior to experimentation in an SPF-level feeding room. The results of subcutaneous afterglow imaging in BALB/c nude mice indicate that **MADBA/TPP** NPs exhibited significant phosphorescence signals, with a high SBR value (28.2). Notably, even 20 seconds after the removal of the UV irradiation, the SBR of the subcutaneous afterglow imaging of **MADBA/TPP** NPs remained as high as 7.6, making the doped material potential for future biological research. To further validate the biosafety of MADBA/TPP NPs and thus support their potential for future applications, we performed corresponding biocompatibility assessments and *in vivo* toxicity evaluations. The CCK-8 method was employed to determine the effect of MADBA/TPP NPs at different concentrations (0, 2.5, 5, 10, and 20 μg mL^{-1}) on the proliferation of mouse fibroblast (L929) cells and human cervical cancer (HeLa) cells. After 24 hours of incubation, the results showed that the viability of both cell types remained above 85% (Fig. 4i), indicating that the NPs exerted no significant cytotoxicity on either normal cells or tumor cells. Subsequently, an *in vivo* acute toxicity study was performed. Specifically, MADBA/TPP NPs at a concentration of 4 mg mL^{-1} (consistent with the concentration used for subcutaneous imaging) were intravenously injected into BALB/c mice. The mice were then maintained for 7 days to allow systemic circulation of the NPs, after which they were euthanized. The major metabolic organs, including the liver, spleen, and kidneys, were harvested for pathological analysis using hematoxylin and eosin (H&E) staining. The H&E images of each organ were observed to be intact, with no signs of toxic damage (Fig. 4j). Collectively, these results demonstrate that MADBA/TPP NPs possess excellent biocompatibility and favorable *in vivo* safety. This provides critical safety assurance for their future application in biomedical research.

Conclusion

In this work, five compounds (triphenylamine, triphenylphosphine, triphenylarsine, triphenylstibine, and triphenylbismuthine) were used as the hosts, and three triphenylamine derivatives were used as the guests to construct doped systems. The heavy atoms contained in the hosts can effectively promote the ISC process of guest excitons, thereby greatly enhancing the phosphorescence emission intensity of the doped materials. The phosphorescence QY gradually increases from 5.2–5.6% in the triphenylbismuthine-based doped materials to 22.8–26.0% in the triphenylbismuth-based doped materials, an astonishing 5.6-fold increase. Theoretical calculations further confirmed that heavy atoms can greatly increase the SOC of hosts, from 1.1 cm^{-1} for triphenylamine to 285.8 cm^{-1} for triphenyltellurium, an increase of up to 259 times. Moreover, the single crystal and XRD analyses of the hosts indicated that heavy atoms endow the hosts with larger spatial volume and good deformability, allowing for better encapsulation of the guests, thereby synergistically enabling the doped materials to show a better phosphorescence performance. Finally, the doped materials with good imaging properties can be effectively used for subcutaneous imaging in mice.

Conflicts of interest

There are no conflicts to declare.

Data availability

The data supporting this article have been included as part of the supplementary information (SI). Supplementary information is available. See DOI: **https://doi.org/10.1039/d5qm00645g**.

CCDC 2481254, 2481255 and 2481256 contain the supplementary crystallographic data for this paper.[50a–c]

Acknowledgements

This work was supported by the National Natural Science Foundation of China (Nos. 52303192 and 22405194). Thanks for the equipment support provided by the Analysis and Testing Center of Peking University, and thanks to Dr Yan Guan for the technical support.

Notes and references

1 B. Fang, L. Lai, M. Fan and M. Yin, Designing organic room temperature phosphorescence with ultralong lifetime by substituent modification, *J. Mater. Chem. C*, 2021, **9**, 11172–11179.
2 Q. Yao, Z. Wang, A. Allam, Z. Da, C. Zhang, J. Wang and M. Wang, In situ synthesis of multicolor phosphorescent films of polyacrylamide by regulating the conjugation of guest molecules, *J. Mater. Chem. C*, 2025, **13**, 12754–12761.
3 C. Li, X. Li and Q. Wang, Supramolecular self-assembling strategy for constructing cucurbit[6]uril derivative-based amorphous pure organic room-temperature phosphorescence complex featuring extra-high efficiency, *Chin. Chem. Lett.*, 2022, **33**, 877–880.
4 H. Sun, Y. Xiao, Y. He, X. Wei, J. Zou, Y. Luo, Y. Wu, J. Zhao, V. K.-M. Au and T. Yu, 3D printable organic room-temperature phosphorescent materials and printed real-time sensing and display devices, *Chem. Sci.*, 2025, **16**, 5299–5309.
5 Y. Guo, R. Pei, J. Qin, W. Chi, J. He, W. Dai, M. Liu, H. Wu, Y. Lei and X. Huang, Precise control of efficient phosphorescence in host–guest doping systems via dynamic metal–ligand coordination, *J. Phys. Chem. Lett.*, 2025, **16**, 537–543.
6 Z. Xu, W. Chen, K. Chen, S. Lin, Z. Wu, G. Deng, J. Chen, M. Tayyab, Y. Xiong, M. D. Li, D. Wang, Z. An and B. Z. Tang, Stimulus-responsive emission via dynamic triplet energy transfer in organic room-temperature phosphorescence glass, *Adv. Mater.*, 2025, **37**, 2418778.
7 Q. Niu, Y. Zhang, Z. Ge, J. Liu, Z. Li, Y. Chen and Y. Liu, Competitive binding based on cucurbit[8]uril for florescence/phosphorescence ratiometric detection of 3-nitrotyrosine, *Chin. Chem. Lett.*, 2025, **36**, 110935.
8 Y. Zhang, H. Li, M. Yang, W. Dai, J. Shi, B. Tong, Z. Cai, Z. Wang, Y. Dong and X. Yu, Organic room-temperature phosphorescence materials for bioimaging, *Chem. Commun.*, 2023, **59**, 5329–5342.
9 H. Zhu, I. Badía-Domínguez, B. Shi, Q. Li, P. Wei, H. Xing, M. C. Ruiz Delgado and F. Huang, Cyclization-promoted ultralong low-temperature phosphorescence via boosting intersystem crossing, *J. Am. Chem. Soc.*, 2021, **143**, 2164–2169.
10 L. Han, H. W. Jin, L. J. Bu, X. Zhang, X. H. Fu, C. Qian, Z. W. Li, Y. Guan, M. X. Chen, Z. M. Ma and Z. Y. Ma, Altering central atoms and bromination sites of phosphorescence units to control ultralong organic room temperature phosphorescence, *Dyes Pigm.*, 2024, **227**, 112186.
11 J. Zhang, E. Sharman, L. Yang, J. Jiang and G. Zhang, Aggregation-induced enhancement of molecular phosphorescence lifetime: a first-principle study, *J. Phys. Chem. C*, 2018, **122**, 25796–25803.
12 L. Ma, M. Cong, S. Sun and X. Ma, Manipulating room-temperature phosphorescence by electron–phonon coupling, *Chem. Sci.*, 2025, **16**, 8282–8290.
13 G. Qu, Y. Zhang and X. Ma, Recent progress on pure organic room temperature phosphorescence materials based on host-guest interactions, *Chin. Chem. Lett.*, 2019, **30**, 1809–1814.
14 X. K. Yao, H. L. Ma, X. Wang, H. Wang, Q. Wang, X. Zou, Z. C. Song, W. Y. Jia, Y. X. Li, Y. F. Mao, M. Singh, W. P. Ye, J. Liang, Y. Y. Zhang, Z. Liu, Y. X. He, J. J. Li, Z. X. Zhou, Z. Zhao, Y. Zhang, G. W. Niu, C. Z. Yin, S. S. Zhang, H. F. Shi, W. Huang and Z. F. An, Ultralong organic phosphorescence from isolated molecules with repulsive interactions for multifunctional applications, *Nat. Commun.*, 2022, **13**, 4890.
15 Y. Xu, Y. Zhu, L. Kong, S. Sun, F. Li, F. Tao, L. Wang and G. Li, Efficient ultralong and color-tunable room-temperature phosphorescence from polyacrylamide platform by introducing sulfanilic acid, *Chem. Eng. J.*, 2023, **453**, 139753.
16 Q. Lou, N. Chen, J. Zhu, K. Liu, C. Li, Y. Zhu, W. Xu, X. Chen, Z. Song, C. Liang, C. X. Shan and J. Hu, Thermally enhanced and long lifetime red tadf carbon dots via multi-confinement and phosphorescence assisted energy transfer, *Adv. Mater.*, 2023, **35**, 2211858.
17 Z. Gong, Q. Cui, X. Nie, G. Zhang and B. Chen, Achieving dual-mode long-persistence afterglow through an aromatic furan organic host–guest system, *Mater. Chem. Front.*, 2025, **9**, 676–683.
18 Z. Wu, J. Nitsch and T. B. Marder, Persistent room-temperature phosphorescence from purely organic molecules and multi-component systems, *Adv. Opt. Mater.*, 2021, **9**, 2100411.
19 M. Han, Z. Xu, J. Lu, Y. Xie, Q. Li and Z. Li, Intramolecular-locked triphenylamine derivatives with adjustable room temperature phosphorescence properties by the substituent effect, *Mater. Chem. Front.*, 2022, **6**, 33–39.
20 S. Li, J. Gu, J. Wang, W. Yuan, G. Ye, L. Yuan, Q. Liao, L. Wang, Z. Li and Q. Li, Excellent persistent near-infrared room temperature phosphorescence from highly efficient host–guest systems, *Adv. Sci.*, 2024, **11**, 2402846.
21 X. Meng, Q. Hu, X. Wang, T. Ma, W. Liu, X. Zhu and C. Ye, Ultralong room-temperature phosphorescence from polycyclic aromatic hydrocarbons by accelerating intersystem crossing within a rigid polymer network, *J. Mater. Chem. C*, 2022, **10**, 17620–17627.
22 L. Ma, S. Sun, B. Ding, X. Ma and H. Tian, Highly efficient room-temperature phosphorescence based on single-benzene structure molecules and photoactivated luminescence with afterglow, *Adv. Funct. Mater.*, 2021, **31**, 2010659.
23 Z. T. Li, B. B. Ding, X. Q. Liu, L. B. Sun and X. Ma, Se/S enhanced room-temperature phosphorescence of organic polymers, *Dyes Pigm.*, 2021, **195**, 109663.
24 M. Fang, J. Yang, X. Xiang, Y. Xie, Y. Dong, Q. Peng, Q. Li and Z. Li, Unexpected room-temperature phosphorescence from a non-aromatic, low molecular weight, pure organic molecule through the intermolecular hydrogen bond, *Mater. Chem. Front.*, 2018, **2**, 2124–2129.
25 H. Wu, D. Wang, J. Zhang, P. Alam, Z. Zhao, Y. Xiong, D. Wang and B. Z. Tang, Achieving persistent room-temperature phosphorescence from phenanthridone derivatives by molecular engineering, *J. Mater. Chem. C*, 2024, **12**, 15527–15534.
26 R. Cen, M. Liu, C. Liu, Q. H. Leng, Q. Ren, Z. Tao and X. Xiao, Nor-seco-Cucurbit[10]uril-based supramolecular assembly for ultralong afterglow room-temperature

phosphorescence material and metal ion detection, *ACS Mater. Lett.*, 2024, **6**, 1992–1998.
27 X. Jiao, W. Zhang, J. Zhi, Y. Wang, M. Wang, Z. Liu and J. Li, Ultra-long organic RTP host–guest doped systems based on pure 4-(1H-imidazole-1-yl)methyl benzoate as versatile hosts, *Mater. Chem. Front.*, 2025, **9**, 1166–1173.
28 Y. Tian, J. Yang, Z. Liu, M. Gao, X. Li, W. Che, M. Fang and Z. Li, Multistage stimulus-responsive room temperature phosphorescence based on host–guest doping systems, *Angew. Chem., Int. Ed.*, 2021, **60**, 20259–20263.
29 J. F. Jiang, J. Q. Liu, C. W. Hu, Y. T. Wang and L. Ma, Construction and fine tuning of host-guest doping systems and the underlying mechanism of room temperature phosphorescence, *Dyes Pigm.*, 2024, **222**, 111931.
30 J. Liu, X. Zhou, X. Tang, Y. Tang, J. Wu, Z. Song, H. Jiang, Y. Ma, B. Li, Y. Lu and Q. Li, Circularly polarized organic ultralong room-temperature phosphorescence: generation, enhancement, and application, *Adv. Funct. Mater.*, 2024, **35**, 2414086.
31 J. Q. Zhao, G. J. Yan, W. Wang, S. S. Shao, B. F. Yuan, Y. J. Li, X. P. Zhang, C. Z. Huang and P. F. Gao, Molecular thermal motion modulated room-temperature phosphorescence for multilevel encryption, *Research*, 2022, **2022**, 9782713.
32 D. Wang, Y. Xie, X. Wu, Y. Lei, Y. Zhou, Z. Cai, M. Liu, H. Wu, X. Huang and Y. Dong, Excitation-dependent triplet–singlet intensity from organic host–guest materials: tunable color, white-light emission, and room-temperature phosphorescence, *J. Phys. Chem. Lett.*, 2021, **12**, 1814–1821.
33 F. M. Xiao, H. Q. Gao, Y. X. Lei, W. B. Dai, M. C. Liu, X. Y. Zheng, Z. X. Cai, X. B. Huang, H. Y. Wu and D. Ding, Guest-host doped strategy for constructing ultralong-lifetime near-infrared organic phosphorescence materials for bioimaging, *Nat. Commun.*, 2022, **13**, 186.
34 L. Wang, J. Zhang, J. Xiong, W. Dai, M. Liu, X. Huang, Y. Chai, Y. Lei, Z. Cai and M. Zhu, Enhancing the phosphorescence performance of organic doped system by carbonylation of guests, *Chin. Chem. Lett.*, 2025, 111706.
35 Z. Zhao, X. Liu, W. Dai, S. Liu, M. Liu, H. Wu, X. Huang and Y. Lei, Enhancing the room-temperature phosphorescence performance by salinization of guests, *J. Phys. Chem. Lett.*, 2024, **15**, 8093–8100.
36 A. Malinge, S. Kumar, D. Chen, E. Zysman-Colman and S. Kéna-Cohen, Heavy Atom effect in halogenated mCP and its influence on the efficiency of the thermally activated delayed fluorescence of dopant molecules, *J. Phys. Chem. C*, 2024, **128**, 1122–1130.
37 M. Li, X. Cai, Z. Chen, K. Liu, W. Qiu, W. Xie, L. Wang and S.-J. Su, Boosting purely organic room-temperature phosphorescence performance through a host–guest strategy, *Chem. Sci.*, 2021, **12**, 13580–13587.
38 J. S. Wang, S. Y. Hu, Y. Y. Wu, Y. T. Zhang, Y. T. Tao and Y. T. Tao, External heavy atom effect in brominated carbazole/oxadiazole hybrid hosts for enhanced efficiency in phosphorescence and TADF OLEDs, *Dyes Pigm.*, 2025, **240**, 112822.
39 H. Deng, G. Li, H. Xie, Z. Yang, Z. Mao, J. Zhao, Z. Yang, Y. Zhang and Z. Chi, Dynamic ultra-long room temperature phosphorescence enabled by amorphous molecular ''Triplet Exciton Pump'' for encryption with temporospatial resolution, *Angew. Chem., Int. Ed.*, 2024, **63**, e202317631.
40 W. Dai, X. Niu, X. Wu, Y. Ren, Y. Zhang, G. Li, H. Su, Y. Lei, J. Xiao, J. Shi, B. Tong, Z. Cai and Y. Dong, Halogen bonding: A new platform for achieving multi-stimuli-responsive persistent phosphorescence, *Angew. Chem., Int. Ed.*, 2022, **61**, e202200236.
41 Y. Lei, J. Yang, W. Dai, Y. Lan, J. Yang, X. Zheng, J. Shi, B. Tong, Z. Cai and Y. Dong, Efficient and organic host–guest room-temperature phosphorescence: tunable triplet–singlet crossing and theoretical calculations for molecular packing, *Chem. Sci.*, 2021, **12**, 6518–6525.
42 Y. Lei, W. Dai, J. Guan, S. Guo, F. Ren, Y. Zhou, J. Shi, B. Tong, Z. Cai, J. Zheng and Y. Dong, Wide-range color-tunable organic phosphorescence materials for printable and writable security inks, *Angew. Chem., Int. Ed.*, 2020, **59**, 16054–16060.
43 J. Guo, C. Hu, J. Liu, Y. Wang and L. Ma, Mechanochromism, tunable pure organic room temperature phosphorescence, single-molecule near-white emission, digital encryption, and anti-counterfeiting, *Dyes Pigm.*, 2024, **221**, 111760.
44 W. Shao, H. Jiang, R. Ansari, P. M. Zimmerman and J. Kim, Heavy atom oriented orbital angular momentum manipulation in metal-free organic phosphors, *Chem. Sci.*, 2022, **13**, 789–797.
45 D. Zhong, S. Liu, L. Yue, Z. Feng, H. Wang, P. Yang, B. Su, X. Yang, Y. Sun and G. Zhou, Achieving pure room temperature phosphorescence (RTP) in phenoselenazine-based organic emitters through synergism among heavy atom effect, enhanced n → π* transitions and magnified electron coupling by the A–D–A molecular configuration, *Chem. Sci.*, 2024, **15**, 9112–9119.
46 X. Liu, Y. Pan, Y. Lei, N. Liu, W. Dai, M. Liu, Z. Cai, H. Wu, X. Huang and Y. Dong, Influence of guest/host morphology on room temperature phosphorescence properties of pure organic doped systems, *J. Phys. Chem. Lett.*, 2021, **12**, 7357–7364.
47 C. Chen, W. Zhang, Z. Wang, X. Wang, J. Yang, Y. Ren, Z. Huang, W. Dai, X. Huang and Y. Lei, Large-area, ultrathin organic films with both photochromic and phosphorescence properties, *Angew. Chem., Int. Ed.*, 2025, **64**, e202501448.
48 S. M. A. Fateminia, Z. Mao, S. Xu, Z. Yang, Z. Chi and B. Liu, Organic nanocrystals with bright red persistent room-temperature phosphorescence for biological applications, *Angew. Chem., Int. Ed.*, 2017, **56**, 12160–12164.
49 S. Cai, H. Shi, D. Tian, H. Ma, Z. Cheng, Q. Wu, M. Gu, L. Huang, Z. An, Q. Peng and W. Huang, Enhancing ultralong organic phosphorescence by effective π-type halogen bonding, *Adv. Funct. Mater.*, 2018, **28**, 1705045.
50 (*a*) CCDC 2481254: Experimental Crystal Structure Determination, 2025, DOI: **10.5517/ccdc.csd.cc2p8ygd**; (*b*) CCDC 2481255: Experimental Crystal Structure Determination, 2025, DOI: **10.5517/ccdc.csd.cc2p8yhf**; (*c*) CCDC 2481256: Experimental Crystal Structure Determination, 2025, DOI: **10.5517/ccdc.csd.cc2p8yjg**.